Natural new particle formation at the coastal Antarctic site Neumayer

R. Weller[1], K. Schmidt[1], K. Teinilä[2], and R. Hillamo[2]

[1] Alfred Wegener Institute for Polar and Marine Research, Am Handelshafen 12, D-27570 Bremerhaven, Germany

[2] Finnish Meteorological Institute, Erik Palménin aukio 1, FI-00101 Helsinki, Finland

Correspondence to: R. Weller (rolf.weller@awi.de)

Abstract

We measured condensation particle (CP) concentrations and particle size distributions at the coastal Antarctic station Neumayer (70°39'S, 8°15'W) during two summer campaigns (from 20 January to 26 March 2012 and 1 February to 30 April 2014) and during polar night between 12 August and 27 September 2014 in the particle diameter (D_p) range from 2.94 nm to 60.4 nm (2012) and from 6.26 nm to 212.9 nm (2014). During both summer campaigns we identified all in all 44 new particle formation (NPF) events. From 10 NPF events, particle growth rates could be determined to be around 0.90±0.46 nm h^{-1} (mean ± std; range: 0.4 nm h^{-1} to 1.9 nm h^{-1}). With the exception of one case, particle growth was generally restricted to the nucleation mode (D_p < 25 nm) and the duration of NPF events was typically around 6.0±1.5 h (mean ± std; range: 4 h to 9 h). Thus in the main, particles did not grow up to sizes required for acting as cloud condensation nuclei. NPF during summer usually occurred in the afternoon in coherence with local photochemistry. During winter, two NPF events could be detected, though showing no ascertainable particle growth. A simple estimation indicated that apart from sulfuric acid, the derived growth rates required other low volatile precursor vapours.

1 Introduction

The crucial role of aerosols as a key component in governing radiation transfer through the Earth's atmosphere and thus their pivotal role in determining climate, has boosted aerosol research activities and strongly promoted our knowledge on this topic. Their relevance in climate forcing is most notably evident since they potentially act as condensation nuclei for cloud droplets, thus influencing radiation transfer indirectly (Haywood and Boucher, 2000; Ramanathan et al., 2001; Carslaw et al., 2013; Rosenfeld et al., 2014). In particular due to the latter effect, involving inherently complicated feedback mechanisms, aerosols still notoriously contribute to the largest uncertainty in estimating climate forcing (for a comprehensive treatise we refer to Boucher et al., 2013 and references therein).

One focus of interest in aerosol research is dedicated to questions regarding new particle formation (NPF), the dominant global particle source generating so-called secondary aerosol (Spracklen et al., 2006). This process starts with the nucleation of gaseous precursors to molecular clusters (Zhang et al., 2012) followed by particle growth to sizes potentially relevant for acting as cloud condensation nuclei (CCN; Spracklen et al., 2008; Bzdek and Johnston, 2010).

Recent research activities documented the global importance of natural secondary aerosol from the marine atmosphere and revealed that apart from dimethyl sulfide (DMS) derived sulfuric acid (H_2SO_4), especially marine volatile organic compounds (VOC) but also reactive iodine species mediate particle nucleation and growth (O'Dowd et al., 2002a and 2002b; Henze and Seinfeld, 2006; O'Dowd and de Leeuw, 2007; Facchini et al., 2008a; McFiggans et al., 2010). Notably in terms of secondary aerosol formation, the virtually completely ice covered and thus effectively source free Antarctic continent represents an outstanding case: Surrounded and isolated by the Southern Ocean from other continents, NPF should be inherently linked with the advection of marine air masses. Apart from some earlier work reporting on the frequent occurrence of bimodal particle size distributions below 100 nm in coastal Antarctica (Ito, 1985 and 1993; Jaenicke et al., 1992), NPF has been recently described for several Antarctic sites. Most extensive measurements were conducted at the

Finnish station Aboa (73°03'S, 13°25'W, 496 m a.s.l.), located on a nunatuk about 130 km from the sea (Koponen et al., 2003; Asmi et al., 2010, Kyrö et al., 2013). Asmi et al. (2010) reported on NPF events showing growth rates (GR) within the nucleation mode between 0.8 nm h^{-1} and 2.5 nm h^{-1}, while in a subsequent summer campaign, significantly higher GR between 1.8 nm h^{-1} and 8.8 nm h^{-1} were found and particle growth usually extended well into the Aitken mode (Kyrö et al., 2013). A thorough data analysis by Kyrö et al. (2013) revealed that most probably biogenic precursors originating from local melting ponds provided low volatile vapour needed for the observed particle growth. Hence this study was the first one indicating that (biogenic) emissions from continental Antarctic could be a source for secondary aerosol formation and relativized the source free character of continental Antarctica. Regarding the Antarctic Plateau, NPF events reported from South Pole were ascribed to local contamination (Park et al., 2004). In contrast, during year-round measurements at Dome C (75°06'S, 123°23'E, 3200 m a.s.l.) several NPF events could be observed throughout the year, mostly associated with particle growth starting from the nucleation into the Aitken mode (Järvinen et al., 2013). Most surprisingly, growth rates tentatively appeared even higher compared to Aboa (median considering all events: 2.5 nm h^{-1}, range: 0.5 nm h^{-1} to 14.1 nm h^{-1}; Järvinen et al., 2013). Finally a recent ship-borne study indicated a Hg driven nucleation event over East Antarctic sea ice (Humphries et al., 2015). Complementary to these local field investigations, dedicated modelling studies can give spatially inclusive and comprehensive insights regarding sources and mechanisms of NPF and the influence on CCN concentrations in the remote atmosphere of the Southern Ocean. Korhonen et al.'s (2008) work revealed a weaker impact of DMS derived secondary aerosol on marine CCN concentrations at high southern latitudes, largely caused by much stronger sea spray emissions south of 45°S. This study also emphasized the importance of NPF in the free troposphere followed by particle growth during entrainment into the marine boundary layer. Yu and Luo's (2010) investigations targeted on modelling DMS derived NPF around coastal Antarctica and demonstrated that ion-mediated nucleation can reasonably predict the observed seasonality of condensation particle (CP) concentrations at coastal Antarctica.

Our present work ties in with a previous publication that examined the climatology of CP concentrations at the German Antarctic research station Neumayer (Weller et al., 2011a). This precedent study indicated the importance of particle nucleation occurring even during late winter and early spring in determining particle number concentrations. In the current study we will entirely focus on the dynamics of particle size distribution and NPF, relying on two dedicated summer campaigns in 2012 and 2014, as well as a measuring period during austral winter (August and September 2014).

2 Experimental techniques and data evaluation methods

2.1 Site description and instrumentation

All experiments were conducted inside the Air Chemistry Observatory located close to Neumayer Station (NM, 70°39' S, 8°15'W, http://www.awi.de/en/science/long-term-observations/atmosphere/antarctic-neumayer/air-chemistry.html, last access: 10 August 2015). Measuring site, prevailing local meteorological conditions, characteristics of the air inlet system, and finally aspects of contamination free sampling have already been described in some detail and we refer to König-Langlo et al. (1998) and Weller et al. (2011a and references therein).

The size distribution of the sub-µm aerosol at NM was determined by a scanning mobility particle sizer (SMPS, TSI classifier model 3080; Wang and Flagan, 1990). During austral summer 2012, i.e. from 20 January through 26 March, the classifier was operated with a so-called nano-DMA (nano differential mobility analyser, TSI Model 3085) in combination with a condensation particle counter (CPC, TSI model WCPC 3788, 50% cut-off diameter $D_{p(50\%)}$ of 2.5 nm). We adjusted aerosol and sheath flow to achieve nominal aerosol size distribution measurements between 2.02 nm and 63.8 nm with a 64 channel resolution. Note that the SMPS primarily measured the electrical mobility of particles which was finally converted by a known transfer function to the corresponding particle mobility diameter D_p. Due to increased uncertainty caused by diffusional losses and cut-off corrections for the used CPC,

we evaluated the data starting from 2.94 nm. All size spectra were multiple charge and diffusion corrected according to the TSI software AIM (Aerosol Instrument Manager®). The original spectra were taken with a scanning time of 120 s (retrace time 15 s) and the average size distribution of 4 consecutive spectra was stored for further evaluation, resulting in a temporal resolution of 600 s (duty cycle 480 s). During 2014 the measuring period was from 1 February through 30 April and from 12 August through 27 September. Due to technical problems we could not run the SMPS with the same configuration as in 2012, but used here a DMA model 3081 in combination with a CPC 3025A (TSI, $D_{p(50\%)}$ of 3 nm). Now, the air flow ratio was adjusted to enable size distribution measurements in the range between 6.26 nm and 212.9 nm. Note that due to the geometry of the DMA 3081, inherently longer particle residence time entailed perceptible particle losses resulting in enhanced uncertainties in the size distribution below 10 nm. As in Dal Maso et al. (2005), we will use the terms nucleation mode for particles with $D_p < 25$ nm and Aitken mode for the size range 25 nm $\leq D_p < 100$ nm throughout the text.

Particle size distributions were evaluated along with continuous long-term condensation particle (CP) concentration measurements (CPC 3022A, TSI, $D_{p(50\%)}$ of 7 nm) and the ionic composition of the aerosol. For the latter, bulk aerosol sampling was regularly conducted in 24-hour time periods using a teflon and a nylon filter in series (all 1 µm pore size). According to Piel et al. (2006) and Weller and Lampert (2008) samples were analyzed by ion chromatography for methane sulfonate ($CH_3SO_3^-$, MSA^-), Cl^-, Br^-, NO_3^-, SO_4^{2-}, Na^+, NH_4^+, K^+, Mg^{2+}, and Ca^{2+}. In addition aerosol light scattering measurements from a continuously operated three-wavelength integrating nephelometer (TSI, type 3563) were considered. Operation and data evaluation were explained in detail in Weller and Lampert 2008. Scattering Ångström exponents α were calculated according to

$$\alpha(\lambda_1 - \lambda_2) = \frac{\log(\sigma_{sp}(\lambda_1)/\sigma_{sp}(\lambda_2))}{\log(\lambda_1/\lambda_2)} \quad (1)$$

where $\alpha(\lambda_1\text{-}\lambda_2)$ refers to the wavelength pair λ_1 (nm) and λ_2 (nm) and $\sigma_{sp}(\lambda)$ are the total scattering coefficients measured in Mm^{-1} (1 Mm^{-1} = 10^{-6} m^{-1}).

Meteorological data were available from the Meteorological Observatory at NM (a description of the observatory itself and the installed meteorological sensors can be found under: http://www.awi.de/nc/en/science/long-term-observations/atmosphere/antarctic-neumayer/meteorology.html, last access: 10 August 2015). The origin of the advected air masses was assessed by 5-day backward trajectories provided by HYSPLIT 4.0 (Hybrid Single-Particle Lagrangian Integrated trajectory; http://www.arl.noaa.gov/documents/reports/hysplit_user_guide.pdf, last access: 10 August 2015). For all trajectory calculations we used GDAS meteorological data with a spatial resolution of 1°×1° (longitude × latitude grid). HYSPLIT trajectories also provide a crude estimate of the vertical mixing height. Calculations were executed in one hour time steps. The accuracy of the used 5-day back trajectories is difficult to assess (see e.g. review by Stohl, 1998). As outlined in Weller et al. (2014) above all the reliability of vertical wind components could be problematic especially for regions like the Southern Ocean with sparse meteorological input data (Harris et al., 2005). Thus we calculated all trajectories using the 3D wind fields of the GDAS data as well as employing the isentropic approximation. We realized in some cases horizontal differences up to around 500 km between the starting points of individual 5-day back trajectories calculated either under 3D or isentropic approximations, but the general horizontal advection characteristic on which our conclusions were finally based appeared robust. As to be expected, the vertical profile could significantly differ between both approaches and should be regarded with particular caution. Finally, in order to specify the characteristics of the local planetary boundary layer (PBL) we additionally gauged vertical mixing in that layer as described in Weller et al. (2011a and 2014) by using the local bulk Richardson number Ri_B (Stull, 1988).

2.2 Data evaluation methods

Particle concentrations, especially within the nucleation mode are susceptible to local contamination. Hence data recorded under potential contamination conditions, indicated by wind directions within a 330°-30° sector and/or wind velocities below 2.0 m s^{-1} were removed. In addition black carbon (BC) concentrations were continuously monitored by a

Multi Angle Absorption Photometer (MAAP model 5012, Thermo Electron Corp.), providing a supplemental criterion for local pollution when BC concentrations levels exceeded 100 ng m^{-3}. Potential contamination happened only very sporadically within short periods (some hours at most) and on the whole, the actual data loss due to potential contamination was virtually negligible.

The crucial point of this study was to identify and characterize new particle formation. For this, we relied on the detailed criteria described by Dal Maso et al. (2005) and Kulmala et al. (2012). According to these recommendations, we defined a NPF event provided that particle size distribution starts within the nucleation mode (D_p < 25 nm) and prevailed for more than an hour. If the recorded size distribution spectra indicated particle growth, the linear growth rate (GR), defined as the change in particle diameter ΔD_p (nm) during a time step Δt (h) was determined by the so-called mode fitting method and in addition by the method of maximum concentration (Dal Maso et al., 2005; Yli-Juuti et al., 2011; Kulmala et al., 2012). We assumed that the GR was constant throughout the event and determined the GR by a linear fit through the geometric mean D_p (derived from the mode fitting procedure) at different times. In our case, nucleation mode and Aitken mode were generally well separated and log-normal distributions could be reliably fitted to the results. In contrast, the maximum concentration method resulted in somewhat higher GR compared to the mode fitting procedure (Table 1, values in parenthesis). However, the latter approach was occasionally not successful thus we relied on the mode fitting method. Finally we estimated nucleation particle formation rate for the size range between 3 nm and 25 nm defined by:

$$J_{3-25} = \frac{UCP_{3-25}}{\Delta t} \qquad (2)$$

Here, $UCP_{3\text{-}25}$ (ultrafine condensation particles) is the particle concentration in the size range between 3 nm and 25 nm derived from the SMPS data. Note that our approach to calculate particle formation as well as GR presumes a homogenous air mass and thus neglects the impact of changing air mass advection. Unfortunately, particle size distribution data were only available from 2.94 nm to 63.8 nm and 6.26 nm to 212.9 nm, respectively, hence an appropriate calculation of coagulation and condensation losses to correct GR and particle

formation rate was impossible, but should usually be negligible in clean, homogeneous air masses (Kulmala et al., 2004a; Leppä et al., 2011). In fact, during both campaigns, total CP concentrations measured by the CPC 3022A were typically below 1000 cm^{-3} and only very rarely reached 2000 cm^{-3}. In addition, during all NPF events nucleation mode particles (D_p < 25 nm) constituted the major component of the total CP concentration. According to Leppä et al. (2011), self-coagulation and coagulation scavenging might have distorted in our case growth rates well below 0.03 nm h^{-1} and 0.02 nm h^{-1}, respectively, corresponding to a condensation sink (CS) < 2×10^{-3} s^{-1}. Virkkula et al. (2011) estimated CS using light scattering data from nephelometer measurements. Adapting the calibration presented therein and the actually observed $\sigma_{sp}(550)$ values during NPF events at NM (typically below 5 Mm^{-1}) indicated again a CS around 10^{-3} s^{-1}.

According to Nieminen et al. (2010) and Yli-Juuti et al. (2011), we finally estimated the H_2SO_4 vapour concentration needed for the calculated GR, assuming that H_2SO_4 was the sole component responsible for the observed particle growth:

$$GR = \frac{\gamma \cdot m_v \cdot v_{mol}}{2\rho} \cdot c_{vapour} \qquad (3)$$

with m_v = molecular mass of the vapour (98 g $mole^{-1}$), ρ = density of the condensed vapour (1.6 g cm^{-3} assuming a H_2SO_4/H_2O mixture), v_{mol} = gas kinetic velocity of the vapour molecules (e.g. 242 m s^{-1} for T = 273 K), c_{vapour} = gaseous H_2SO_4 concentration (mole cm^{-3}) to be determined, and γ is close to the H_2SO_4 accommodation coefficient (assumed to be around 1.0).

3 Results

3.1 Data presentation

During the first summer campaign in 2012 (comprising 66 observation days and 9500 raw spectra) we identified 19 events of NPF without clearly discernible particle growth (class II events according to Dal Maso et al., 2005). Growth rates could be reliably determined in 8

class I or so-called "banana-type" events (Dal Maso et al., 2005). An overview of size resolved aerosol data for the months January through March 2012 as well as a selected series of consecutive NPF events is presented in the Supplementary Material (Figs. S.1 and S.2) together with concurrently measured total CP concentrations, meteorological parameters, and the ionic composition of the bulk aerosol (data from both campaigns reported here are available at http://dx.doi.org/10.1594/PANGAEA.845024). Figure 1 focuses on a striking NPF event happened on January 27, where a simultaneous nucleation- and Aitken mode growth was evident. This NPF event will be further discussed as case study in 4.1. Figure 2 shows a more detailed topographic view of this event on a linear dN/dlogDp scale and is supplemented by corresponding profiles of log-normal distribution fits from selected time slices. In addition, a strikingly prolonged Aitken mode growth over about 3 days (GR = 0.3±0.05 nm h^{-1}) started at 1 March (doy 61) but without exhibiting a discernible nucleation mode (Supplementary Material, Fig. S.2). Particle concentrations in the nucleation mode were strongly correlated with total CP concentrations measured by the CPC 3022A (Supplementary Material, Fig. S.1b). A correlation of particle concentrations measured by the SMPS in the range between 5 nm and 64 nm with CP concentrations revealed a linear dependence (slope 0.992, r^2 = 0.8; see Fig. S.3 in the Supplementary Material), indicating that during summer CP number concentrations were dominated by nucleation and Aitken mode particles.

In contrast, the yield of NPF events during summer 2014 (February through April 2014, 85 observation days, 12240 raw spectra) was rather scanty: Apart from 15 class II events, only 2 class I events could be discerned. A presentation of this time series can again be found in the Supplementary Material (Fig. S.4). During winter (August and September 2014, 37.5 observation days, 5370 raw spectra), two certain class II events were evident (14/15 August and 21 September, Fig. 3). Figure 4 presents the mean particle size distribution during both winter events and for comparison for a typical non-event day (18 August 2014). Table 1 summarizes all evaluated class I events and lists the calculated GR, nucleation particle formation rates ($J_{3\text{-}25}$) and the estimated H_2SO_4 concentration hypothetically needed for the respective GR.

3.2 Meteorological aspects

Regarding local meteorology, virtually all NPF events observed at NM occurred during southerly wind directions (180°±60°) with wind velocities below 12 m s^{-1} (typically between 4 m s^{-1} and 8 m s^{-1}). Usually bright weather conditions prevailed with a cloud amount below 3 Octans and a relative sun shine duration around (48±26)% relating to clear sky conditions, except for three NPF events occurring during cloud covered sky (25 February 2012, 08 and 09 March 2012). In all cases the local PBL was characterized by Ri_B numbers < 0.25, indicating turbulent flow and a well-mixed PBL. This was supported by HYSPLIT back trajectory analyses indicating vertical mixing heights around 250 m (range: 100 m to 600 m) for the last 6 hours before arrival at NM (5-day back trajectories for the most prominent nucleation events are presented in the Supplementary Material, Fig. S.5). Note, however that mixing heights provided by HYSPLIT should be treated as a rough estimate, particularly regarding the Antarctica PBL due to the impact of katabatic winds and uncertain vertical wind components in general. The spatial extend of NPF events associated with appreciable particle growth could be estimated to be around 170±85 km, taking into account the prevailing wind velocity (around 8±4 m s^{-1}) and the confined NPF duration (around 6 hours, Table 1). Backward trajectories for NPF events revealed that frequently air masses originated from the marine boundary layer (MBL) of the South Atlantic and then typically travelled along the Antarctic coastline up to five days before arrival at NM (Supplementary Material Fig. S.5). A subsequent contact time of these trajectories with open water or sea ice was rather limited and often happened, if at all, just some hours before arrival at NM. During NPF events trajectories mainly stayed below 1500 m above ground for the last 48 hours before arrival at NM and mainly within the vertical mixing heights derived from HYSPLIT for the last 24 hours. Only for the NPF event at 16 March 2012 air masses clearly descended from the free troposphere (in this case >2000 m above ground) within the last 24 hours before arrival at NM. In summary, NPF related trajectories did neither indicate a pronounced impact of recent MBL air advection nor of descending air masses from the free troposphere. Hence they appeared somewhat equivocal in evaluating a rather local process like NPF, probably because of their particularly inherent spatial uncertainty in a region sparsely supported by meteorological data.

During summer, nucleation events showed a distinct diurnal cycle. They typically occurred in the second half of the day indicating a link to local photochemistry, though being sometimes delayed to the diurnal maximum of UV radiation by a few hours (Figs. 1 and S.2; Table 1). We did not discover a meaningful relation between UV irradiance and GR or particle formation rate. Table 2 presents a comparison of selected auxiliary parameters during NPF and non-event days. In summary, NPF events tend to be accompanied by drier air (impact of southerly, continental advection), lower aerosol light scattering coefficients (indicating lower particle surface area), and less aerosol mass. Winter events happened either several hours around midnight or more than day-long (Fig. 3) and the measured maximum UV radiance was 4 W m^{-2} and 18 W m^{-2} for the NPF event observed on August and September, respectively. Again, respecting 5-day back trajectories documented a similar advection pattern as for the summertime NPF events (Supplementary Material Fig. S.6).

During stormy weather, occasionally enhanced particle concentrations appeared below 10 nm. In this context, it is worth to mention that Virkkula et al. (2007) and Asmi et al. (2010) observed at Aboa some nucleation events associated with high wind speeds and suggested ion production by fast moving ice crystals followed by subsequent ion-mediated nucleation. As for NM the situation was somewhat unclear, because charged particle concentration data were not available and during stormy weather the overall electrostatic charge in combination with inherently critical electrical grounding conditions on ice may have provoked instrumental artefacts.

4 Discussion

4.1 Case study

A striking series of NPF occurred during three days, starting around noon at 26 January 2012 with a class II event (Fig. 1a), accompanied by an immediate increase of $UCP_{3\text{-}25}$ concentration (Fig. 1b). Around noon two size distribution maxima were discernible below 25 nm, one around 6 nm, the other between 15 nm and 20 nm. While the first one disappeared

after 16:00 UTC, the latter lingered on and started to grow between 07:00 and 14:00 UTC next day (GR = 1.9 nm h^{-1}, Table 1), finally reaching a mode maximum around 50 nm after a further growth during the afternoon of 28 January 2012. Coinciding with particle growth, the difference between CP and UCP_{3-25} concentrations steeply increased due to particle formation in the size range D_p > 25 nm. Starting at 11:00 UTC on 27 January 2012 a class I NPF event was observed showing particle growth from around 7 nm to 20 nm during the following 7 hours. Particle growth started again during the afternoon of 28 January 2012 eventually reaching a mode maximum around 25 nm (Fig. 1a and Fig. 2).

Interestingly, this class I NPF event commenced immediately after a striking peak in light scattering coefficients (Fig. 1d). Given that nephelometer measurements are primarily sensitive to particle concentrations within a size range comparable to the measuring wavelengths, this peak indicated simultaneously enhanced accumulation mode particle concentrations. One may argue that enhanced accumulation mode particles acted as additional CS and inhibited NPF, but this would be inconsistent to the observed distinct growth of the 15 nm nucleation mode from the previous day already starting at 07:00 UTC. Concerning meteorological and radiation conditions, all three days were virtually cloudless (as can also be deduced from the smooth and nearly sinusoidal $UV_{300-370}$ signal, Fig. 1d) and southerly advection dominated. Trajectory analyses revealed that air masses had actually no contact with the MBL for at least 48 hours before, but most of them originated in the MBL of the South Atlantic (Fig. 5) about 5 days before. This finding suggested a long range transport of marine precursor gases associated with a delayed nucleation just before arrival at NM. Except a short period around 02:00 UTC at 28/01/2012, Ri_B values indicated a well-mixed boundary layer (Fig. 1c).

From the measured size distribution spectra we calculated the total aerosol mass concentration m_p between 3 nm and 64 nm, assuming a particle density of 1.8 g cm^{-3} (according to pure H_2SO_4 as an upper limit for dry sulfuric acid aerosol). The result is presented in Fig. 1e together with the ionic composition of the aerosol derived from our daily aerosol sampling. MSA^- and nss-SO_4^{2-} mass concentrations increased throughout, while those of Na^+ (a tracer for sea salt aerosol) and NH_4^+ remained low (note that the time of the filter exchange is

marked with vertical red lines). The stepwise increase of m_p appeared roughly comparable to the increase of nss-SO_4^{2-} mass concentrations from day to day. Note, that this estimate presumes pure sulfuric acid aerosol and should thus be treated as upper limit assessment. Furthermore, based on our measurements we cannot finally deduce whether H_2SO_4 vapour genuinely condensed on freshly formed nucleation mode particles or merely on aged background aerosol.

4.2 Extent of particle growth

In view of previous results from Antarctica (Asmi et al., 2010, Järvinen et al., 2013; Kyrö et al., 2013), NPF at NM appeared notably less efficient. Particle growth was usually confined to the nucleation mode and only once extended into the Aitken mode (see case study described in 4.1). Consequently, this NPF event was the only one at NM where the growth of nucleated particles reached a size range potentially relevant for acting as CCN. On the other hand, a persistent, but not locally developed Aitken mode was often present during polar day (Supplementary Material S.1) and after being missing in August reappeared in September (Fig. 3). Notwithstanding, some discrete events with strikingly high particle concentrations between 30 nm and 200 nm occurred in August exclusively under stormy weather (wind velocity around 20 m s^{-1}; Fig. 3). Contemporaneously, Na^+ concentrations increased from back-ground levels around 80 ng m^{-3} to values between 480 ng m^{-3} and 1010 ng m^{-3}. According to impactor measurements conducted by Teinilä et al. (2014) in the year 2010 at NM, most probably sub-µm sea salt aerosol might also have caused the latter peculiarities.

4.3 Role of DMS derived sulfuric acid and MSA

Although air mass advection pattern assessed by trajectory calculations turned out to be equivocal, the observed diurnal cycle of NPF and the ionic composition of the aerosol indicate that particle nucleation at NM was most probably induced by emissions of marine biogenic precursor gases (Yu and Luo, 2010). More precisely, photo-oxidation of phytoplankton derived dimethyl sulfide (DMS) is in general the prominent photochemical process in the troposphere of coastal Antarctica (e.g. Minikin et al., 1998), yielding ultimately

sulfuric acid (H_2SO_4) and methane sulfonic acid (MSA, CH_3SO_3H). Nevertheless, and in agreement with results from other Antarctic sites (Järvinen et al., 2013; Kyrö et al., 2013), H_2SO_4 concentrations needed for the observed growth rates should be at least an order of magnitude higher compared to available values actually observed in Antarctica: Jefferson et al. (1998) measured mean H_2SO_4 concentrations around 1.6×10^6 molec cm^{-3} during the SCATE campaign at Palmer Station (Antarctic Peninsula) in summer, and at South Pole during the ISCAT 2000 campaign H_2SO_4 (MSA) concentrations around 0.27×10^6 molec cm^{-3} (0.08×10^6 molec cm^{-3}) were detected in December (Mauldin III et al., 2004). Although the chemical composition of secondary aerosol during summer at NM was usually dominated by DMS derived nss-SO_4^{2-} and MS (Weller and Lampert 2008; Weller et al., 2011b), according to this estimate observed particle growth in the early stage should yet be controlled by other low volatile vapours.

4.4 Possible role of H_2O vapour, NH_3, organic vapour, and iodine oxide

Theoretical and laboratory studies revealed that H_2O molecules are important for early particle growth (2-3 nm) due to stabilization of the critical nucleus by H_2SO_4-hydrate formation, while further particle growth is dominated by H_2SO_4 or low volatile organic vapours (Nieminen et al., 2010; Zhang et al., 2012). These investigations indicated that under prevalent atmospheric conditions nucleation rate might be correlated with relative humidity (rH), depending on NH_3 and organic vapour concentrations (Zhang et al., 2012). Concerning this point, our data were inconclusive: It seems, though in contrast to the above mentioned investigations, that NPF events sometimes occurred during rH decrease (Supplementary Material, Fig. S.2). But this apparent correlation was particularly due to the fact that we mainly observed NPF in the afternoon when increasing temperatures usually induced decreasing rH levels. In addition, a correlation between H_2O vapour partial pressure (i.e. absolute humidity) and nucleation rates derived from equation (1) was absent.

Apart from H_2SO_4 and H_2O vapour, gaseous precursors like NH_3, organic vapours (notably organic amines), and inorganic iodine compounds (mainly iodine oxides) are known to be strongly involved in particle nucleation and particle growth (O'Dowd et al., 2002b; Kulmala

et al., 2004b; Facchini et al., 2008a; McFiggans et al., 2010; Metzger et al., 2010; Benson et al., 2011; Dawson et al., 2012; Riccobono et al., 2012; Riipinen et al., 2012; Wang et al., 2013). As for NH_3, previous thermodenuder measurements at NM indicated that biogenic secondary aerosol was likely an internal mixture of the acids H_2SO_4 and MSA partly neutralized by NH_3 (Weller et al., 2011a). Actually, we observed NH_4^+ concentrations at NM of around 10 ng m^{-3}. Preliminary results on the amount of water soluble organic carbon (WSOC, excluding MSA), determined from bulk filter samples taken during austral summer 2011 showed values between 5 and 35 ngC m^{-3} (method: solid phase extraction followed by TOC analysis; Lehmann, personal communication 2015). Interestingly, NH_4^+ and WSOC concentrations appeared thus similar to values reported from Aboa (Asmi et al., 2010) where particle growth was more pronounced. At Aboa, biogenic emissions by nearby melting ponds were found to be a potential source for condensable vapour (Kyrö et al., 2013), while the surroundings of NM are completely ice covered throughout (apart from open water dependent on seasonal sea ice coverage) and the nearest insular rocky outcrops are more than 200 km away. One may speculate that marine primary organic aerosol was dominant at NM, linked with sea spray formation by bubble bursting (Facchini et al., 2008b), while at Aboa condensable organic vapour emissions from melting ponds were decisive.

From the mid-latitude European sites Roscoff and Mace Head there exists strong evidence for iodine mediated NPF (O'Dowd et al., 2002b; McFiggans et al., 2010) and in recent studies, a possible impact of IO on NPF in the Arctic (Allan et al., 2014) and particle number concentrations at Halley Station, Antarctica (Roscoe et al., 2015) were inferred. Concerning iodine compounds, in situ measurements by long-path Differential Optical Absorption Spectroscopy (LP-DOAS) conducted at Halley (Saiz-Lopez et al., 2007) as well as respective satellite observations (Schönhardt et al., 2012) revealed maximum IO concentration of some 5 pptv (volume parts per trillion) over Antarctic coastal regions around October. Such IO levels were comparable to coastal European sites like Roscoff and Mace Head (O'Dowd et al., 2002b; McFiggans et al., 2010). At NM, multi-axis (MAX) DOAS measurements using scattered skylight primarily provided IO column densities, which did not show a discernible seasonality (Frieß et al., 2010). Note that MAX-DOAS measurements were only available

during clear sky conditions and solar zenith angles < 85° and were not available regarding the observed winter NPF events. Presuming that IO was restricted within the PBL (below 2 km), comparable IO mixing ratios in the range of some pptv could be derived for NM in some cases, but this approach is actually highly uncertain (Frieß et al., 2001 and 2010). Interestingly, at Dumont d'Urville (DDU), IO concentrations were found to be an order of magnitude lower indicating that halogen chemistry in general was probably promoted by the much larger sea ice extend of the Atlantic sector of Antarctica (Grilli et al., 2013). Considering the available laboratory-, field- and model results, it appears difficult to estimate IO concentrations needed to provoke significant particle nucleation but it seems that several pptv IO or OIO would be necessary (Pechtl et al., 2006; Saiz-Lopez et al., 2012; Roscoe et al., 2015). In view of the minor importance of DMS photochemistry, however, we speculate that IO probably initiated the observed NPF at NM in late winter. The shape of both winter events and the fact that growth rates could not be determined indicated a local origin where particle size distribution developed during transport time to the measuring site (Kulmala et al., 2012).

5 Conclusions

In summary, based on ancillary data NPF events were most likely mediated by $H_2SO_4/NH_3/H_2O$ ternary nucleation during summer at NM, while the observed particle growth was governed by the availability of other yet not identified gaseous precursors, most probably low volatile organic compounds of marine origin. Due to the apparent deficit of the latter, particle growth was accordingly restricted within the nucleation mode and in the main did not extend to particle diameter ranges relevant for acting as cloud condensation nuclei. Given that particle growth in the early stage (i.e. within the nucleation mode) was governed by low volatile vapours other than H_2SO_4, another remaining crucial question is, in which way the finally sulfuric acid dominated secondary aerosol at NM was ultimately generated. During summer, a potential role of iodine oxides in particle nucleation was unclear, while for the observed winter events these compounds could be potential candidates. But then, the even

more pronounced deficit of condensable vapour due to depressed photochemical activity impeded particle growth beyond particle diameters of about 15 nm.

In conclusion, our investigations indicate three crucial points concerning NPF in Antarctica that are supposed to be addressed in future work: (i) Up to now, from this region only sparse and inadequate knowledge exists on organic aerosols, in particular secondary organic aerosol. Identification of the most important compounds, their origin and source strength is still fragmentary at best. (ii) IO concentrations should be measured year-round by in-situ techniques in order to better assess its role in NPF and validate respecting satellite retrievals. (iii) The role of free tropospheric air in providing gaseous precursor for particle nucleation and growth within the PBL needs clarification. This point appeared especially important for continental Antarctica in view of the recently described NPF events observed at Dome C (Järvinen et al., 2013).

Acknowledgements

The authors would like to thank the technicians and scientists of the Neumayer overwintering teams of the years 2012 and 2013, whose outstanding commitment enabled continuous high quality measurements. RH and KT thank Academy of Finland for the financial support (project ACPANT, decision nr 264375). Special thanks go to Kathrin Höppner, responsible for the Air Chemistry Observatory during the overwintering 2012, to Udo Frieß for beneficial discussions respecting IO concentrations at NM, and finally to Astrid Lampert for many fruitful suggestions. We are thankful to NOAA Air Resources Laboratory for having made available the HYSPLIT trajectory calculation program as well as all used input data files.

References

Allan, J. D., Williams, P. I., Najera, J., Whitehead, J. D., Flynn, M. J., Taylor, J. W., Liu, D., Darbyshire, E., Carpenter, L. J., Chance, R., Andrews, S. J., Hackenberg, S. C., and McFiggans, G.: Iodine observed in new particle formation events in the Arctic atmosphere during ACCACIA, Atmos. Chem. Phys., 15, 5599-5609, doi:10.5194/acp-15-5599-2015, 2015.

Asmi, E., Frey, A., Virkkula, A., Ehn, M., Manninen, H.E., Timonen, H., Tolonen-Kivimäki, O., Aurela, M., Hillamo, R., and Kulmala, M.: Hygroscopicity and chemical composition of Antarctic sub-micrometer aerosol particles and observations of new particle formation, Atmos. Chem. Phys., 10, 4253-4271, doi:10.5194/acp-10-4253-2010, 2010.

Benson, D. R., Yu, J. H., Markovich, A., and Lee, S.-H.: Ternary homogeneous nucleation of H_2SO_4, NH_3, and H_2O under conditions relevant to the lower troposphere, Atmos. Chem. Phys., 11, 4755-4766, doi:10.5194/acp-11-4755-2011, 2011.

Boucher, O., Randall, D., Artaxo, P., Bretherton, C., Feingold, G., Forster, P., Kerminen, V.-M., Kondo, Y., Liao, H., Lohmann, U., Rasch, P., Satheesh, S.K., Sherwood, S., Stevens B., and Zhang, X.Y.: Clouds and Aerosols. In: Climate Change 2013: The Physical Science Basis. Contribution of Working Group I to the Fifth Assessment Report of the Intergovernmental Panel on Climate Change [Stocker, T.F., Qin, D., Plattner, G.-K., Tignor, M., Allen, S.K., Boschung, J., Nauels, A., Xia, Y., Bex V., and Midgley P.M. (eds.)]. Cambridge University Press, Cambridge, United Kingdom and New York, NY, USA, 2013.

Bzdek, B. and Johnston, M.V.: New Particle Formation and Growth in the Troposphere, Anal. Chem., 82, No. 19, 7871-7878, doi:10.1021/ac100856j, 2010.

Carslaw, K.S., Lee, L.A., Reddington, C.L., Pringle, K.J., Rap, A., Forster, P.M., Mann, G.W., Spracklen, D.V., Woodhouse, M.T., Regayre, L.A. and Pierce, J.R.: Large contribution of natural aerosol to uncertainty in indirect forcing, Nature, 503, 67-71, doi:10.1038/nature12674, 2013.

Dal Maso, M., Kulmala, M., Riipinen, I., Wagner, R., Hussein, T., Aalto, P.P., and Lehtinen, E.J.: Formation and growth of fresh atmospheric aerosols: eight years of aerosol size distribution data from SMEAR II, Hyytiälä, Finland, Boreal Env. Res., 10, 323-336, 2005.

Dawson, M.L., Varner, M.E., Perraud, V., Ezell, M.J., Gerber, R.B., and Finlayson-Pitts, B.J.: Simplified mechanism for new particle formation from methanesulfonic acid, amines, and water via experiments and ab initio calculations, PNAS, 109 (46), 18719-18724, doi:10.1073/pnas.1211878109, 2012.

Facchini, M.C., Decesari, S., Rinaldi, M., Carbone, C., Finessi, E., Mircea, M., Fuzzi, S., Moretti, F., Tagliavini, E., Ceburnis, D., and O'Dowd, C.D.: Important Source of Marine Secondary Organic Aerosol from Biogenic Amines, Environ. Sci. Technol., 42 (24), 9116-9121, 2008a.

Facchini, M.C., Rinaldi, M., Decesari, S., Carbone, C., Finessi, E., Mircea, M., Fuzzi, S., Ceburnis, D., Flanagan, R., Nilsson, E.D., de Leeuw, G., Martino, M., Woeltjen, J., and O'Dowd, C.D.: Primary submicron marine aerosol dominated by insoluble organic colloids and aggregates, Geophys. Res. Lett., 35, L17814, doi:10.1029/2008GL034210, 2008b.

Frieß, U., Wagner, T., Pundt, I., Pfeilsticker, K., and Platt, U.: Spectroscopic Measurements of Troposheric Iodine Oxide at Neumayer Station, Antarctica, Geophys. Res. Lett., 28, 1941-1944, doi:10.1029/2000GL012784, 2001.

Frieß, U., Deutschmann, T., Gilfedder, B. S., Weller, R., and Platt, U.: Iodine monoxide in the Antarctic snowpack, Atmos. Chem. Phys., 10, 2439-2456, doi:10.5194/acp-10-2439-2010, 2010.

Grilli, R., Legrand, M., Kukui, A., Méjean, G., Preunkert, S., and Romanini, D.: First investigations of IO, BrO, and NO_2 summer atmospheric levels at a coastal East Antarctic site using mode-locked cavity enhanced absorption spectroscopy, Geophys. Res. Lett., 40, 791-796, doi:10.1002/grl.50154, 2013.

515 Harris, J.M., Draxler, R.R., and Oltmans, S.J.: Trajectory model sensitivity to differences in
516 input data and vertical transport method, J. Geophys. Res., 110, D14109,
517 doi:10.1029/2004JD005750, 2005.

518 Haywood, J. and Boucher, O.: Estimates of the direct and indirect radiative forcing due to
519 tropospheric aerosols: A review, Rev. Geophys., 38(4), 513-543, 2000.

520 Henze, D.K. and Seinfeld, J.H.: Global secondary organic aerosol from isoprene oxidation,
521 Geophys. Res. Lett., 33, L09812, doi:10.1029/2006GL025976, 2006.

522 Humphries, R. S., Schofield, R., Keywood, M., Ward, J., Pierce, J. R., Gionfriddo, C. M.,
523 Tate, M., Krabbenhoft, D., Galbally, I. E., Molloy, S. B., Klekociuk, A., Johnston, P. V.,
524 Kreher, K., Thomas, A. J., Robinson, A. D., Harris, N. R. P., Johnson, R., and Wilson, S. R.:
525 Boundary layer new particle formation over East Antarctic sea ice – possible Hg driven
526 nucleation?, Atmos. Chem. Phys. Discuss., 15, 19477-19536, doi:10.5194/acpd-15-19477-
527 2015, 2015.

528 Ito, T.: Study of background aerosols in the Antarctic Troposphere, J. Atmos. Chem. 3, 69-91,
529 1985.

530 Ito, T.: Size distribution of Antarctic submicron aerosols, Tellus, 45B, 145-159, 1993.

531 Jaenicke, R., Dreiling, V., Lehmann, E., Koutsenoguii, P.K., and Stingl, J.: Condensation
532 nuclei at the German Antarctic Station „Georg von Neumayer“, Tellus, 44B, 311-317, 1992.

533 Järvinen, E., Virkkula, A., Nieminen, T., Aalto, P. P., Asmi, E., Lanconelli, C., Busetto, M.,
534 Lupi, A., Schioppo, R., Vitale, V., Mazzola, M., Petäjä, T., Kerminen, V.-M., and Kulmala,
535 M.: Seasonal cycle and modal structure of particle number size distribution at Dome C,
536 Antarctica, Atmos. Chem. Phys., 13, 7473-7487, doi:10.5194/acp-13-7473-2013, 2013.

537 Jefferson, A., Tanner, D.J., Eisele, F.L., Davis, D.D., Chen, G., Crawford, J., Huey, J.W.,
538 Torres, A.L., and Berresheim, H: OH photochemistry and methane sulfonic acid formation in
539 the coastal Antarctic boundary layer, J. Geophys. Res., 103(D1), 1647-1656, 1998.

540 König-Langlo, G., King, J.C., Pettré, P.: Climatology of the three coastal Antarctic stations
541 Dumont d’Urville, Neumayer and Halley, J. Geophys. Res., 103(D9), 10,935-10,946, 1998.

Koponen, I.K., Virkkula, A., Hillamo, R., Kerminen, V.-M., Kulmala, M.: Number size distribution and concentrations of the continental summer aerosol in Queen Maud Land, Antarctica, J. Geophys. Res., 108(D18), 4587, doi:10.1029/2003JD003614, 2003.

Korhonen, H., Carslaw, K.S., Spracklen, D.V., Mann, G.W., and Woodhouse, M.T.: Influence of oceanic dimethyl sulfide emissions on cloud condensation nuclei concentrations and seasonality over the remote Southern Hemisphere oceans: A global model study, J. Geophys. Res., 113(D15204), doi:10.1029/2007JD009718, 2008.

Kulmala, M., Vehkamäki, H., Petäjä, T., Dal Maso, M., Lauri, A., Kerminen, V.-M., Birmili, W., McMurry, P.H.: Formation and growth rates of ultrafine atmospheric particles: a review of observations, Aerosol Sci., 35, 143-176, doi:10.1016/j.jaerosci.2003.10.003, 2004a.

Kulmala, M., Kerminen, V.-M., Anttila, T., Laaksonen, A., and O'Dowd, D: Organic aerosol formation via sulphate cluster activation, J. Geophys. Res., 109 (D04205, doi:10.1029/2003JD003961, 2004b.

Kulmala, M., Petäjä, T., Nieminen, T., Sipilä, M., Manninen, H.E., Lehtipalo, K., Dal Maso, M., Aalto, P.P., Junninen, H., Paasonen, P., Riipinen, I., Lehtinen, K.E.J., Laaksonen, A., and Kerminen, V.-M.: Measurements of the nucleation of atmospheric aerosol particles. Nature Protocols, Vol.7 No.9, 1651-1667, doi:10.1038/nprot.2012.091, 2012.

Kyrö, E.-M., Kerminen, V.-M., Virkkula, A., Dal Maso, M., Parshintsev, J., Ruíz-Jimenez, J., Forsström, L., Manninen, H. E., Riekkola, M.-L., Heinonen, P., and Kulmala, M.: Antarctic new particle formation from continental biogenic precursors, Atmos. Chem. Phys., 13, 3527-3546, doi:10.5194/acp-13-3527-2013, 2013.

Leppä, J., Anttila, T., Kerminen, V.-M., Kulmala, M., and Lehtinen, K. E. J.: Atmospheric new particle formation: real and apparent growth of neutral and charged particles, Atmos. Chem. Phys., 11, 4939-4955, doi:10.5194/acp-11-4939-2011, 2011.

Mauldin III, R.L., Kosciuch, E., Henry, B., Eisele, F.L., Shetter, R., Lefer, B., Chen, G., Davis, D., Huey, G., Tanner, D.: Measurements of OH, HO_2+RO_2, H_2SO_4, and MSA at the South Pole during ISCAT 2000, Atmos. Environ., 38, 5423-5437, 2004.

McFiggans, G., Bale, C.S.E., Ball, S.M., Beames, J.M., Bloss, W.J., Carpenter, L.J., Dorsey, J., Dunk, Flynn, M.J., Furneaux, K.L., Gallagher, M.W., Heard, D.E., Hollingsworth, A.M., Hornsby, K., Ingham, T., Jones, C.E., Jones, R.L., Kramer, L.J., Langridge, J.M., Leblanc, C., LeCrane, J.-P., Lee, J.D., Leigh, R.J., Longley, I., Mahajan, A.S., Monks, P.S., Oetjen, H., Orr-Ewing, A.J., Plane, J.M.C., Potin, P., Shillings, A.J.L., Thomas, F., von Glasow, R., Wada, R., Whalley, L.K., and Whitehead, J.D.: Iodine-mediated coastal particle formation: an overview of the Reactive Halogens in the Marine Boundary Layer (RHaMBLe) Roscoff coastal study, Atmos. Chem. Phys., 10, 2975-2999, 2010.

Metzger, A., Verheggen, B., Dommen, J., Duplissy, J., Prevot, A.S.H., Weingartner, E., Riipinen, I., Kulmala, M., Spracklen, D.V., Carslaw, K.S., and Baltensperger, U.: Evidence for the role of organics in aerosol particle formation under atmospheric conditions, PNAS, 107 (15), 6646-6651, doi:10.1073/pnas.0911330107, 2010.

Minikin, A., Legrand, M., Hall, J., Wagenbach, D., Kleefeld, C., Wolff, E., Pasteur, E.C. and Ducroz, F.: Sulfur-containing species (sulfate and methanesulfonate) in coastal Antarctic aerosol and precipitation, J. Geophys. Res., 103(D9), 10 975-10 990, 1998.

Nieminen, T., Lehtinen, K. E. J., and Kulmala, M.: Sub-10 nm particle growth by vapor condensation – effects of vapor molecule size and particle thermal speed, Atmos. Chem. Phys., 10, 9773-9779, doi:10.5194/acp-10-9773-2010, 2010.

O'Dowd, C.D. and de Leeuw, G.: Marine aerosol production: a review of the current knowledge, Phil. Trans. R. Soc. A, 365, 1753-1774, doi:10.1098/rsta.2007.2043, 2007.

O'Dowd, C.D., Hämeri, K., Mäkelä, J.M., Pirjola, L., Kulmala, M., Jennings, S.G., Berresheim, H., Hansson, H.-C., de Leeuw, G., Kunz, G.J., Allen, A.G., Hewitt, C.N., Jackson, A., Viisanen, Y., and Hoffmann, T.: A dedicated study of New Particle Formation and Fate in the Coastal Environment (PARFORCE): Overview of objectives and achievements. J. Geophys. Res., 107(D19), 8108, doi:10.1029/2001JD000555, 2002a.

O'Dowd, C.D., Jimenez, J.L., Bahreini, R., Flagan, R.C., Seinfeld, J.H., Hämeri, K., Pirjola, L., Kulmala, M., Jennings, S.G., Hoffmann, T.: Marine aerosol formation from biogenic iodine emissions, Nature, 417, 632-636, doi:10.1038/nature00775, 2002b.

597 Park, J., Sakurai, H., Vollmers, K., McMurry, P.H.: Aerosol size distributions measured at
598 South Pole during ISCAT, Atmos. Environ., 38, 5493-5500,
599 doi:10.1016/j.atmosenv.2002.12.001, 2004.

600 Pechtl, S., Lovejoy, E.R., Burkholder, J.B., and von Glasow, R.: Modeling the possible role of
601 iodine oxides in atmospheric new particle formation, Atmos. Chem. Phys., 6, 505-523,
602 doi:10.5194/acp-6-505-2006, 2006.

603 Piel, C., Weller, R., Huke, M. and Wagenbach, D.: Atmospheric methane sulfonate and non-
604 sea salt sulphate records at the EPICA deep-drilling site in Dronning Maud Land, Antarctica,
605 J. Geophys. Res., 111(D03304), doi:10.1029/2005JD006213, 2006.

606 Ramanathan, V., Crutzen, P.J., Kiehl, J.T., Rosenfeld, D.: Aerosols, Climate, and the
607 Hydrological Cycle, Science, 294, 2119-2124, 2001.

608 Riccobono, F., Rondo, L., Sipilä, M., Barmet, P., Curtius, J., Dommen, J., Ehn, M., Ehrhart,
609 S., Kulmala, M., Kürten, A., Mikkilä, J., Paasonen, P., Petäjä, T., Weingartner, E., and
610 Baltensperger, U.: Contribution of sulfuric acid and oxidized organic compounds to particle
611 formation and growth, Atmos. Chem. Phys., 12, 9427-9439, doi:10.5194/acp-12-9427-2012,
612 2012.

613 Riipinen, I., Yli-Juuti, T., Pierce, J.R., Petäjä, T., Worsnop, D.R., Kulmala, M., and Donahue,
614 N.M.: The contribution of organics to atmospheric nanoparticle growth, Nature Geoscience,
615 5, 453-458, doi:10.1038/ngeo1499, 2012.

616 Roscoe, H.K., Jones, A.E., Brough, N., Weller, R., Saiz-Lopez, A., Mahajan, A.,
617 Schoenhardt, A., Burrows, J.P., Fleming, Z.L.: Particles and iodine compounds in coastal
618 Antarctica, J. Geophys. Res. Atmos., 120, doi:10.1002/2015JD023301, 2015.

619 Rosenfeld, D., Andreae, M.O., Asmi, A., Chin, M., de Leeuw, G., Donovan, D.P., Kahn, R.,
620 Kinne, S., Kivekäs, N., Kulmala, M., Lau, W., Schmidt, K.S., Suni, T., Wagner, T., Wild, M.,
621 and Quaas, J.: Global observations of aerosol-cloud-precipitation-climate interactions, Rev.
622 Geophys., 52, doi:10.1002/2013RG000441, 2014.

623 Saiz-Lopez, A., Mahajan, A.S., Salmon, R.A., Bauguitte, J.-B., Jones, A.E., Roscoe, H.K.,
624 and Plane, J.M.C.: Boundary Layer Halogens in Coastal Antarctica, Science, 317, 348-351,
625 doi:10.1126/science.1141408, 2007.

626 Saiz-Lopez, A., Plane, J.M.C., Baker, A.R., Carpenter, L.J., von Glasow, R., Gómez Martin,
627 J.C., McFiggans, G., and Saunders, R.W.: Atmospheric Chemistry of Iodine, Chem. Rev., 112
628 (3), 1773-1804, doi:10.1021/cr200029u, 2012.

629 Schönhardt, A., Begoin, M., Richter, A., Wittrock, F., Kaleschke, L., Gómez Martín, J. C.,
630 and Burrows, J. P.: Simultaneous satellite observations of IO and BrO over Antarctica,
631 Atmos. Chem. Phys., 12, 6565-6580, doi:10.5194/acp-12-6565-2012, 2012.

632 Spracklen, D. V., Carslaw, K. S., Kulmala, M., Kerminen, V.-M., Mann, G. W., and Sihto, S.-
633 L.: The contribution of boundary layer nucleation events to total particle concentrations on
634 regional and global scales, Atmos. Chem. Phys., 6, 5631-5648, doi:10.5194/acp-6-5631-2006,
635 2006.

636 Spracklen, D. V., Carslaw, K. S., Kulmala, M., Kerminen, V.-M., Sihto, S.-L., Riipinen, I.,
637 Merikanto, J., Mann, G. W., Chipperfield, M. P., Wiedensohler, A., Birmili, W., Lihavainen,
638 H.: Contribution of particle formation to global cloud condensation nuclei concentrations,
639 Geophys. Res. Lett., 35, L06808, doi:10.1029/2007GL033038, 2008.

640 Stohl, A.: Computation, accuracy and applications of trajectories-a review and bibliography,
641 Atmos. Environ., 32(6), 947-966, 1998.

642 Stull, R.B.: An Introduction to Boundary Layer Meteorology, Kluwer Academic Publishers,
643 Dordrecht, Dordrecht, 175-180, 1988.

644 Teinilä, K., Frey, A., Hillamo, R., Tülp, H.C., and Weller, R.: A study of the sea-salt
645 chemistry using size-segregated aerosol measurements at coastal Antarctic station Neumayer,
646 Atmos. Environ., 96, 11-19, 2014.

647 Virkkula, A., Hirsikko, A., Vana, M., Aalto, P.P., Hillamo, R., and Kulmala, M.: Charged
648 particle size distributions and analysis of particle formation events at the Finnish Antarctic
649 research station Abao, Boreal Environ. Res., 12, 397-408, 2007.

650 Virkkula, A., Backman, J., Aalto, P. P., Hulkkonen, M., Riuttanen, L., Nieminen, T., dal
651 Maso, M., Sogacheva, L., de Leeuw, G., and Kulmala, M.: Seasonal cycle, size dependencies,
652 and source analyses of aerosol optical properties at the SMEAR II measurement station in
653 Hyytiälä, Finland, Atmos. Chem. Phys., 11, 4445-4468, doi:10.5194/acp-11-4445-2011,
654 2011.

655 Wang, S.C. and Flagan, R.C.: Scanning Electrical Mobility Spectrometer, Aerosol Sci.
656 Technol., 13,230-240, 1990.

657 Wang, J., McGraw, R. L., and Kuang, C.: Growth of atmospheric nano-particles by
658 heterogeneous nucleation of organic vapor, Atmos. Chem. Phys., 13, 6523-6531,
659 doi:10.5194/acp-13-6523-2013, 2013.

660 Weller, R., and Lampert, A.: Optical properties and sulfate scattering efficiency of boundary
661 layer aerosol at coastal Neumayer Station, Antarctica, J. Geophys. Res., 113, D16208,
662 doi:10.1029/2008JD009962, 2008.

663 Weller, R., Minikin, A., Wagenbach, D., and Dreiling, V.: Characterization of the inter-
664 annual, seasonal, and diurnal variations of condensation particle concentrations at Neumayer,
665 Antarctica, Atmos. Chem. Phys., 11, 13243-13257, doi:10.5194/acp-11-13243-2011, 2011a.

666 Weller, R., Wagenbach, D, Legrand, M., Elsässer, C., Tian-Kunze, X., and König-Langlo, G.:
667 Continuous 25-years aerosol records at coastal Antarctica – 1: inter-annual variability of ionic
668 compounds and links to climate indices, Tellus, 63B, 901-919, doi: 10.1111/j.1600-
669 0889.2011.00542.x, 2011b.

670 Weller, R., Levin, I., Schmithüsen, D., Nachbar, M., Asseng, J., and Wagenbach, D.: On the
671 variability of atmospheric ^{222}Rn activity concentrations measured at Neumayer, coastal
672 Antarctica, Atmos. Chem. Phys., 14, 3843-3853, doi:10.5194/acp-14-3843-2014, 2014.

673 Yli-Juuti, T., Nieminen, T., Hirsikko, A., Aalto, P. P., Asmi, E., Hõrrak, U., Manninen, H. E.,
674 Patokoski, J., Dal Maso, M., Petäjä, T., Rinne, J., Kulmala, M., and Riipinen, I.: Growth rates
675 of nucleation mode particles in Hyytiälä during 2003−2009: variation with particle size,

676 season, data analysis method and ambient conditions, Atmos. Chem. Phys., 11, 12865-12886,
677 doi:10.5194/acp-11-12865-2011, 2011.

678 Yu, F. and Luo, G.: Oceanic Dimethyl Sulfide Emission and New Particle Formation around
679 the Coast of Antarctica: A Modeling Study of Seasonal Variations and Comparison with
680 Measurements, Atmosphere, 1, 34-50, doi:10.3390/atmos1010034, 2010.

681 Zhang, R., Khalizov, A., Wang, L., Hu, M., and Xu, W.: Nucleation and Growth of
682 Nanoparticles in the Atmosphere, Chem. Rev., 112, 1957-2011, doi:10.1021/cr2001756,
683 2012.

Table 1. Nucleation events of class I (Dal Maso et al., 2005) during austral summer 2012 and 2014: Time period during which the particle growth in the given range was observed, growth rate determined by log normal mode fitting and maximum concentration (in parenthesis) method, particle formation rate in the size range 3 nm to 25 nm ($J_{3\text{-}25}$), and estimated H_2SO_4 vapour concentration needed for the observed growth rate.

Date (doy 2012)	Time period	Growth rate (nm h^{-1})	Range (nm)	$J_{3\text{-}25}$ (cm^{-3} s^{-1})	H_2SO_4 needed (molec cm^{-3})
27 Jan 2012 (27)	07:00–14:00	1.9±0.1 (2.5±0.3)	18.7 – 33.7	0.1 ± 0.05	7.3×10^7
	11:00–18:00	1.8±0.1 (2.1±0.3)	6.8 – 20.2	n.d.*	6.6×10^7
23 Feb. 2012 (54)	12:00–18:00	0.6±0.07 (n.d.)	4.9 – 8.9	0.1 ± 0.03	2.4×10^7
25 Feb. 2012 (56)	13:00–17:00	0.9±0.07 (n.d.)	5.2 – 8.4	0.03 ± 0.01	3.3×10^7
27 Feb. 2012 (58)	11:00–18:00	1.0±0.05 (1.1±0.2)	11.6 – 18.5	0.06 ± 0.02	3.7×10^7
	13:00-18:00	0.9±0.09 (1.0±0.2)	5.2 – 9.1	0.06 ± 0.02	3.7×10^7
08 Mar. 2012 (68)	08:00–17:00	0.8±0.04 (1.0±0.1)	7.8 – 14.8	0.02 ± 0.01	3.2×10^7
09 Mar. 2012 (69)	14:00–19:00	0.8±0.08 (1.4±0.3)	5.2 – 9.1	0.08 ± 0.03	3.7×10^7
16 Mar. 2012 (76)	10:00–16:00	0.8±0.1 (1.5±0.6)	13.2 – 18.3	0.07 ± 0.02	3.0×10^7
	14:00-21:00	1.0±0.09 (1.1±0.2)	5.9 – 12.9	0.09 ± 0.03	1.8×10^7
24 Mar. 2012 (84)	15:00–19:00	0.5±0.05 (n.d.)	4.1 – 6.1	0.02 ± 0.01	2.7×10^7
06 Feb. 2014	14:00–19:00	0.4±0.2‡ (n.d.)	8.8 – 11.3‡	n.d.†	1.5×10^7
24 Mar. 2014	11:00–18:00	0.5±0.1 (n.d.)	14.5 – 16.6	n.d.†	1.7×10^7

* n.d. = not determined
‡ measured with the long DMA (TSI model 3081) with enhanced uncertainty below 10 nm
† particle formation rate not determined due to higher cut-off of the SMPS used during this period

Table 2. Comparison of selected meteorological and aerosol light scattering parameters as well as ionic composition of the aerosol (all items in mean ± std) during days with NPF as characterized in Table 2 and non-event days. The comparison is restricted to the summer months (January through March).

parameter	NPF event	non-event
relative humidity (%)	77.9±4.7	82.4±5.1
$p(H_2O)$ (hPa)	262±98	281±100
$\sigma_{sp}(450)$ (Mm^{-1})	2.30±0.9	3.20±2.2
$\sigma_{sp}(550)$ (Mm^{-1})	1.65±0.7	2.50±1.9
$\sigma_{sp}(700)$ (Mm^{-1})	1.30±0.5	2.00±1.5
$\alpha_{sc}(450\text{-}550)$	1.8±0.2	1.4±0.2
$\alpha_{sc}(450\text{-}700)$	1.4±0.2	1.3±0.2
$\alpha_{sc}(550\text{-}700)$	1.2±0.2	1.3±0.3
MSA^- (ng m^{-3})	109±54	132±100
nss-SO_4^{2-} (ng m^{-3})	225±67	274±160
Na^+ (ng m^{-3})	45±19	79±130
NH_4^+ (ng m^{-3})	6.6±3	12.5±11

Figure captions

Figure 1. Time series of the measured particle size distribution dN/dlogDp (cm^{-3}) on a logarithmic scale (color code to the right of the contour plot) of NPF events around 27 January 2012 showing a growing nucleation and Aitken mode (a), corresponding CP concentration (black line) and particle concentrations between 3 nm and 25 nm ($UCP_{3\text{-}25}$, red line) (b), wind velocity (red line), wind direction (black line) and Ri_B (bue line) (c), light scattering coefficients σ_{sp} at 450 nm, 550 nm, and 700 nm (blue, green and red lines) as well as UV radiation at wavelengths between 300 nm and 370 nm (purple line) (d), aerosol mass m_p derived from SMPS measurements assuming a density of 1.8 g cm^{-3}, as well as MSA^-, nss-SO_4^{2-}, Na^+, and NH_4^+ concentrations derived from daily aerosol samples (red lines mark the time of filter exchange) (e).

Figure 2. Detailed presentation of the NPF event around 27 January 2012 with a linear dN/dlogDp (cm^{-3}) scale as z-axis, based on hourly mean SMPS data recorded with 64 channel resolution. The lower panel shows exemplarily six log-normal distribution fits through size distributions measured at 27 January between 12:00 and 17:00. The mode mean diameters (in nm) are noted next to the respecting modal maxima.

Figure 3. Time series of particle size distribution dN/dlogDp (cm^{-3}) measured during winter 2014 (12 August through 27 September, logarithmic color code to the right of the contour plot) (a), CP concentration (b), wind velocity (red line) and wind direction (black line) (c). The yellowish shaded areas in (c) mark stormy weather conditions associated with snow drift.

Figure 4. Mean size distribution (red line) and range of geometric standard deviation (grey envelope) during both winter particle nucleation events (15/16 August and 21 September 2014), as well as for typical winter day without nucleation (18 August 2012).

Figure 5. Five-day back trajectories based on 3D wind fields for the period 26 January 2012 through 28 January 2012: Horizontal advection pattern (a) and vertical profiles (b). Trajectories which arrived around the main NPF events (noon on 26 and 27 January 2012) are plotted as bold lines.

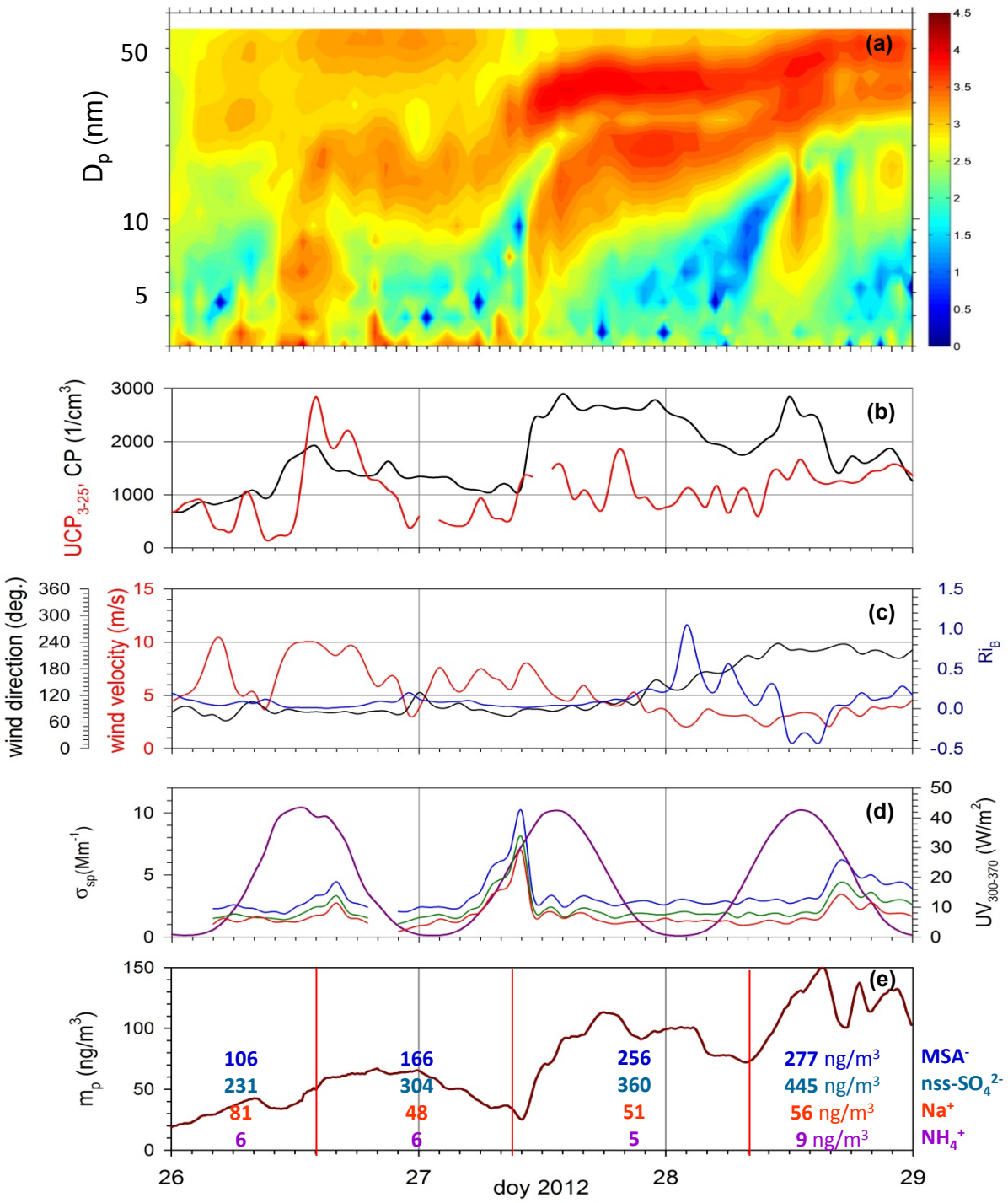
(a)
D_p (nm)
50
10
5
4.5
4
3.5
3
2.5
2
1.5
1
0.5
0
(b)
$UCP_{3\text{-}25}$, CP (1/cm^3)
3000
2000
1000
0
(c)
wind direction (deg.)
360
300
240
180
120
60
0
wind velocity (m/s)
15
10
5
0
Ri_B
1.5
1.0
0.5
0.0
-0.5
(d)
σ_{sp}(Mm^{-1})
10
5
0
$UV_{300\text{-}370}$ (W/m^2)
50
40
30
20
10
0
(e)
m_p (ng/m^3)
150
100
50
0
106
231
81
6
166
304
48
6
256
360
51
5
277 ng/m^3
445 ng/m^3
56 ng/m^3
9 ng/m^3
MSA$^-$
nss-SO_4^{2-}
Na^+
NH_4^+
26
27
28
29
doy 2012

Figure 1

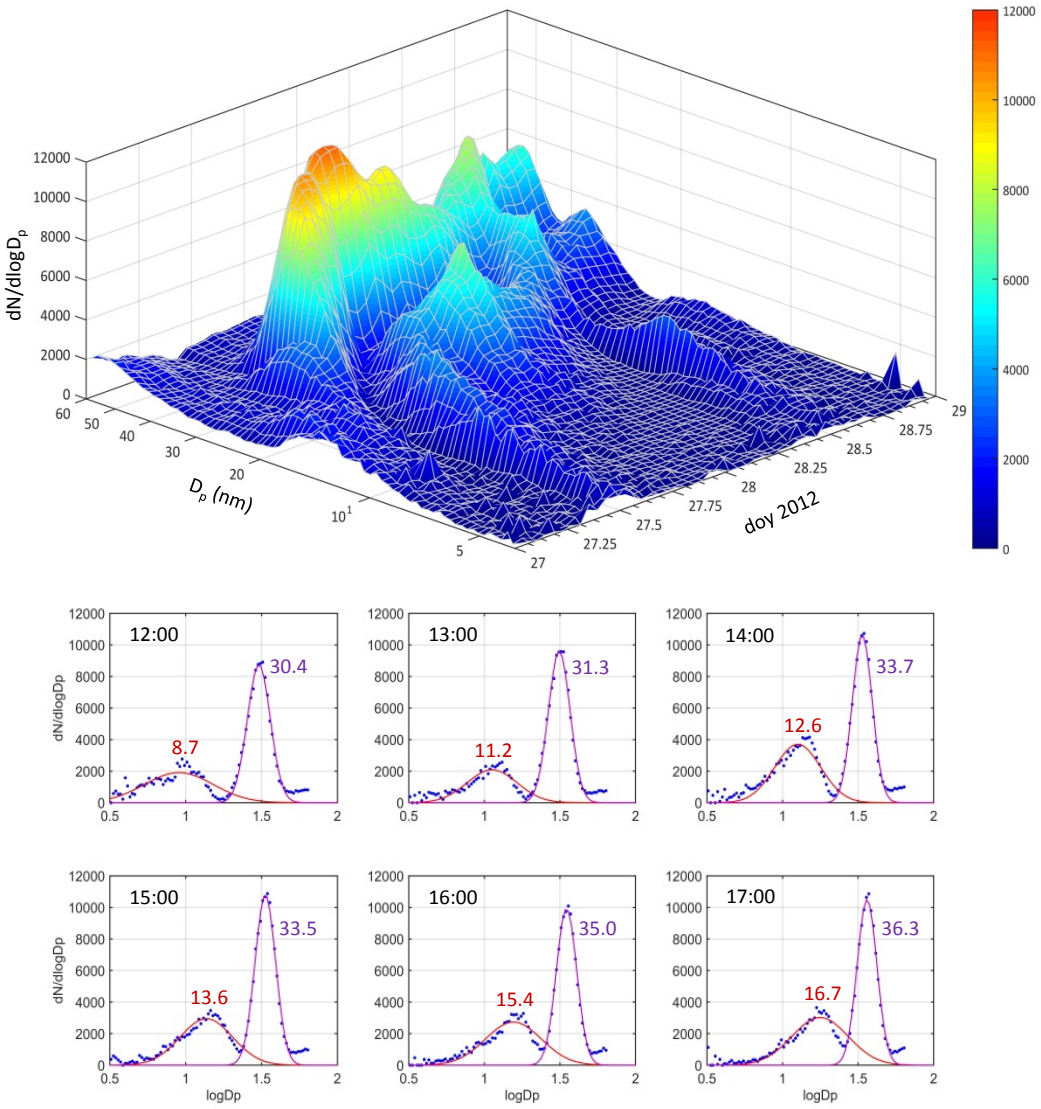
dN/dlogDp
Dp (nm)
doy 2012
12:00
30.4
8.7
13:00
31.3
11.2
14:00
33.7
12.6
15:00
33.5
13.6
16:00
35.0
15.4
17:00
36.3
16.7
logDp

Figure 2

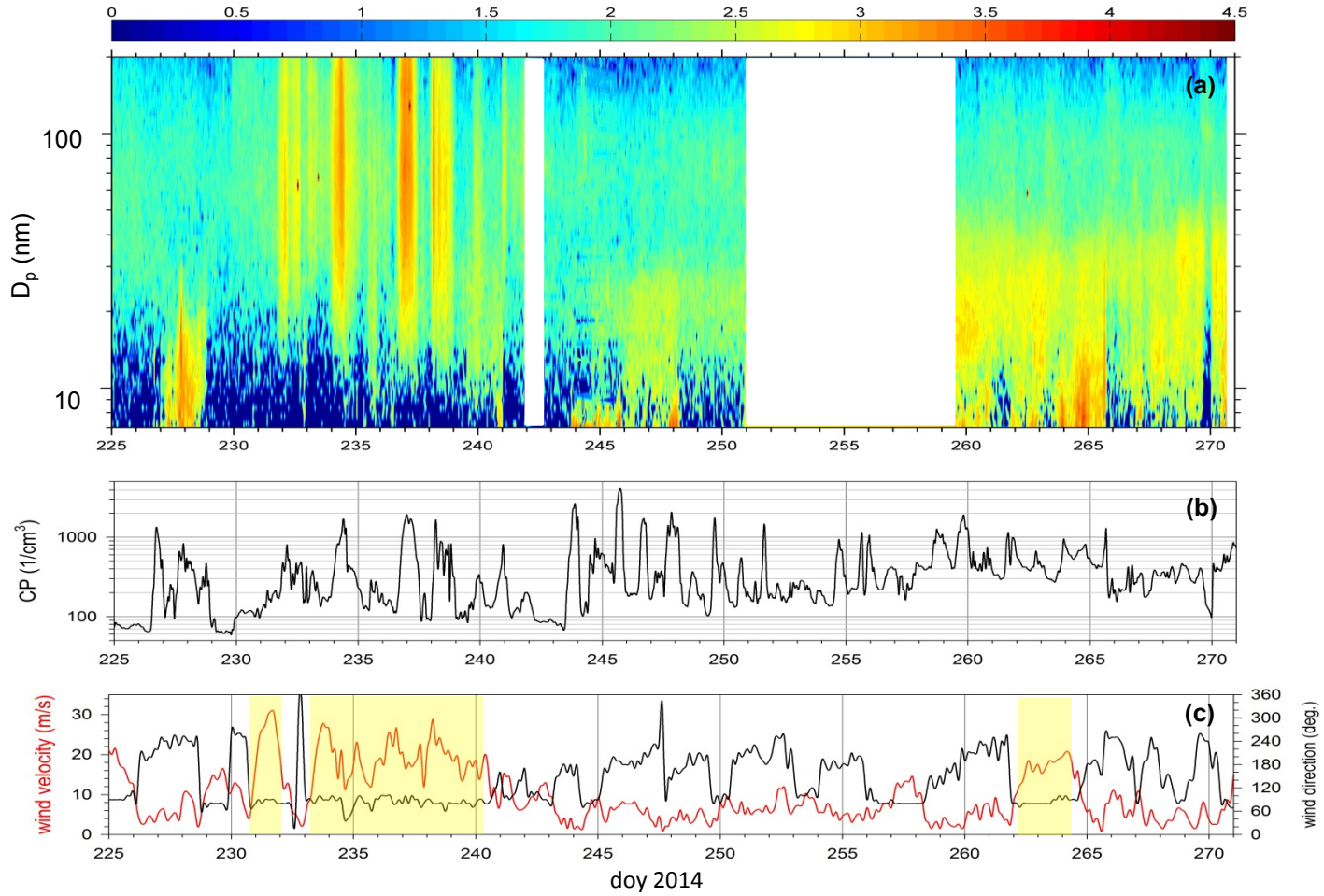
0
0.5
1
1.5
2
2.5
3
3.5
4
4.5
(a)
100
10
D_p (nm)
225
230
235
240
245
250
255
260
265
270
(b)
CP (1/cm^3)
1000
100
(c)
wind velocity (m/s)
30
20
10
0
360
300
240
180
120
60
0
wind direction (deg.)
doy 2014

Figure 3

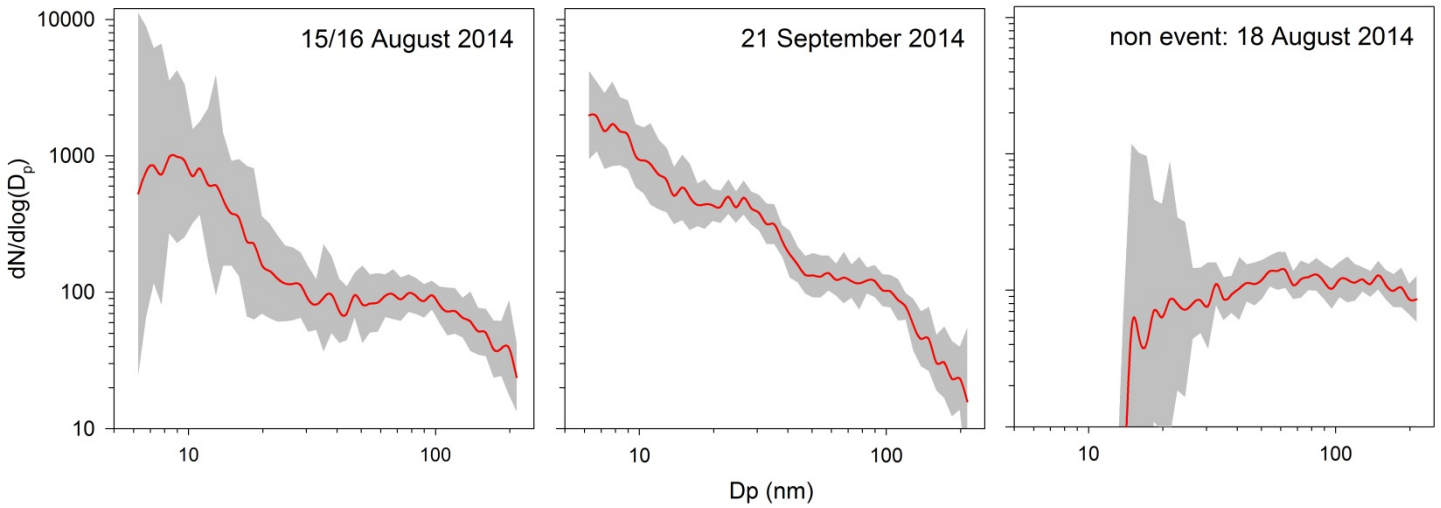
15/16 August 2014
21 September 2014
non event: 18 August 2014
dN/dlog(D$_p$)
10000
1000
100
10
10
100
Dp (nm)

Figure 4

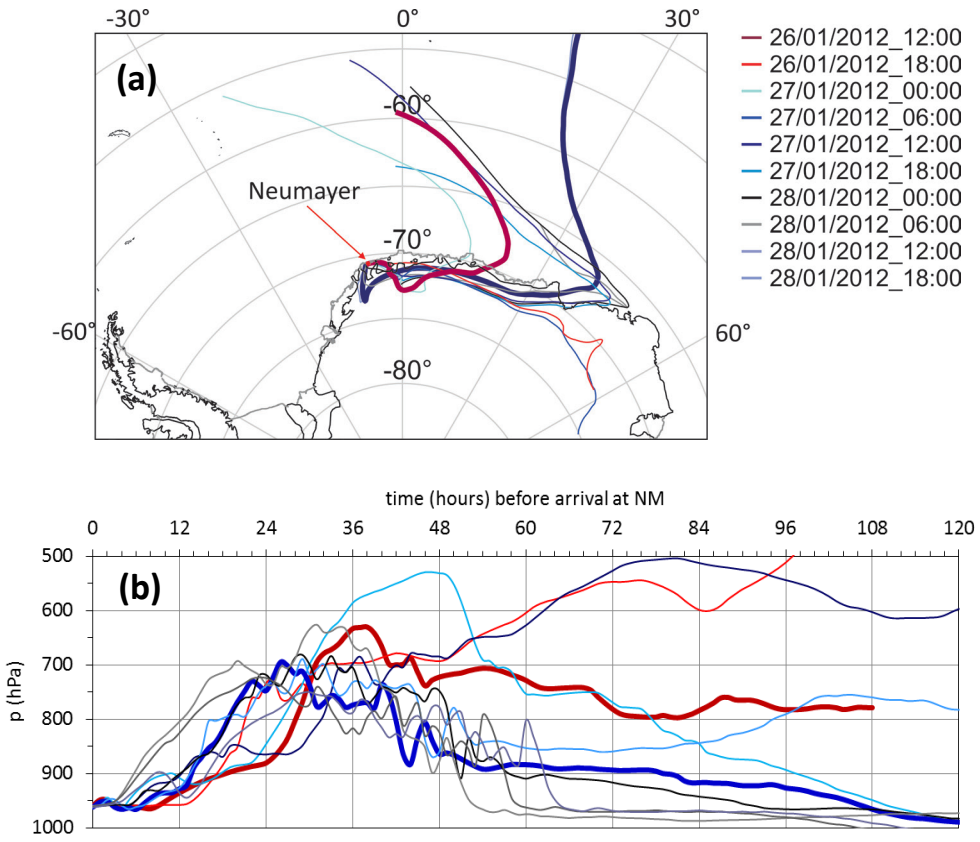
(a)
-30°
0°
30°
-60°
-70°
-80°
-60°
60°
Neumayer
26/01/2012_12:00
26/01/2012_18:00
27/01/2012_00:00
27/01/2012_06:00
27/01/2012_12:00
27/01/2012_18:00
28/01/2012_00:00
28/01/2012_06:00
28/01/2012_12:00
28/01/2012_18:00
(b)
time (hours) before arrival at NM
0
12
24
36
48
60
72
84
96
108
120
p (hPa)
500
600
700
800
900
1000

Figure 5